

Differential cross sections for electron impact excitation of Xe: I. Excitation of the five lowest levels; experiment and theory

M A Khakoo[†], S Trajmar^{†‡}, L R LeClair^{†‡||}, I Kanik^{†‡}, G Csanak^{†§} and C J Fontes^{†§}

[†] Department of Physics, California State University, Fullerton, CA 92634, USA

[‡] Jet Propulsion Laboratory, California Institute of Technology, Pasadena, CA 91109, USA

[§] Los Alamos National Laboratory, University of California, Los Alamos, NM 87544, USA

Received 7 March 1996

Abstract. Experimental and theoretical differential cross sections (DCSs) for electron impact excitation of the five lowest levels of xenon are reported. The experimental data were obtained at impact energies of 10, 15, 20 and 30 eV for scattering angles in the range of 0° to 135°. The scattering intensities for excitation of various levels with respect to that of the combined two lowest levels (representing the corresponding DCS ratios) were measured with conventional electrostatic electron energy-loss spectrometers. Absolute DCSs for excitation of the combined two lowest levels were derived from DCS ratios for excitation of the combined two lowest levels and elastic scattering and utilizing the elastic DCSs of Register *et al.* These DCS ratios were obtained from scattering intensity ratios measured with conventional electrostatic electron energy-loss spectrometers after correction for instrumental effects by utilizing electron time-of-flight measurements for determining the proper value of this ratio at 90° scattering angle for each impact energy. The unitarized first-order many-body theory and the unitarized distorted-wave approximation were applied to obtain the theoretical differential cross sections for impact energies of 10, 15, 20, 30, 50 and 80 eV. The present experimental and theoretical results are compared with each other and with other available experimental and theoretical DCSs.

1. Introduction

The present study, concerning differential cross sections (DCSs) for electron impact excitation of Xe, was motivated by the need for such data both for testing the accuracy and reliability of theoretical methods and for providing data for practical applications. Xenon, being the heaviest of the rare gases, is expected to pose a severe test to theoretical methods aimed at calculating these cross sections and to represent tedious and difficult measurements due to the strong dependence of the DCSs on impact energy and scattering angle. The predominant practical application of Xe DCSs is for modelling in plasma and laser physics (see, e.g., Rhodes 1983). Some examples of additional practical applications include electroluminescence in xenon-gas proportional scintillation counters (Novgorodov 1974), plasma display panel technology (Williamson *et al* 1994, Veerasingam *et al* 1995) and tokamak fusion research (Tawara and Phaneuf 1988).

|| NRC Resident Research Associate.

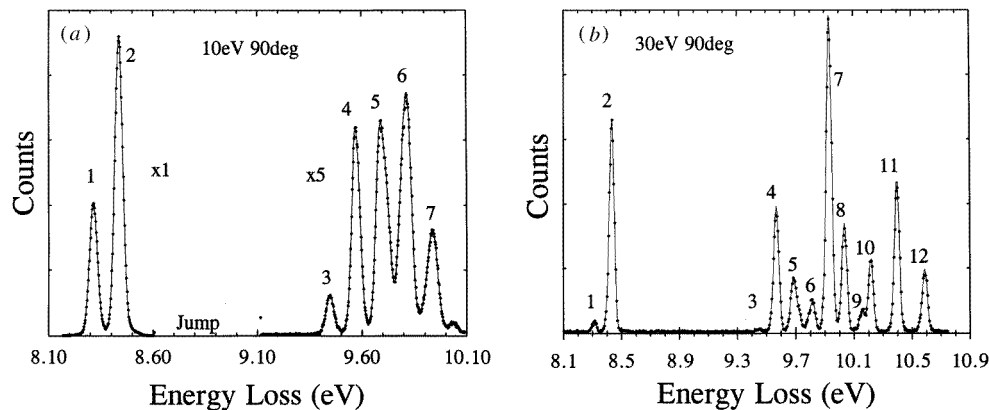


Figure 1. Electron energy-loss spectra of xenon. (a) $E_0 = 10$ eV and $\theta = 90^\circ$. (b) $E_0 = 30$ eV and $\theta = 90^\circ$. Both the experimental data (dots) and the fitted spectra (curves) are shown. The designation of the energy-loss features is indicated in accordance with table 1.

Table 1. Designation of energy-loss features in terms of level excitations. The level energies from Moore (1957) and from our calculations are also given.

E-loss feature no	Level no	Level designation	Energy (eV) (Moore)	Energy (eV) (LANL)	Dominant configurations and levels
0	0	$5p^6\ ^1S_0$	0.000	0.000	$0.998(5p^6\ ^1S_0) + \dots$
1	1	$6s[\frac{3}{2}]_2$	8.315	8.361	$0.996(5p^56s\ ^3P_2) + \dots$
2	2	$6s[\frac{3}{2}]_1$	8.437	8.458	$0.777(5p^56s\ ^1P_1) + 0.626(5p^56s\ ^3P_1) + \dots$
3	3	$6s'[\frac{1}{2}]_0$	9.447	9.537	$0.906(5p^56s\ ^3P_0) + 0.413(5p^55d\ ^3P_0) + \dots$
4	4	$6s'[\frac{1}{2}]_1$	9.570	9.618	$0.72(5p^56s\ ^3P_1) - 0.61(5p^56s\ ^1P_1) + 0.33(5p^55d\ ^3P_1) + \dots$
	5	$6p[\frac{1}{2}]_1$	9.580	9.577	$0.86(5p^56p\ ^3S_1) - 0.46(5p^56p\ ^3P_1) + 0.21(5p^56p\ ^1P_1) + \dots$
5	6	$6p[\frac{5}{2}]_2$	9.686	9.675	$0.70(5p^56p\ ^3D_2) + 0.68(5p^56p\ ^1D_2) - 0.21(5p^56p\ ^3P_2) + \dots$
	7	$6p[\frac{5}{2}]_3$	9.721	9.689	$0.9997(5p^56p\ ^3D_3) + \dots$
6	8	$6p[\frac{3}{2}]_1$	9.789	9.754	$0.76(5p^56p\ ^1P_1) + 0.48(5p^56p\ ^3P_1) - 0.44(5p^56p\ ^3D_1) + \dots$
	9	$6p[\frac{3}{2}]_2$	9.821	9.773	$0.88(5p^56p\ ^3P_2) + 0.45(5p^56p\ ^1D_2) - 0.18(5p^56p\ ^3D_2) + \dots$
7	10	$5d[\frac{1}{2}]_0$	0.891	9.992	$0.90(5p^55d\ ^3P_0) - 0.42(5p^56s\ ^3P_0) + \dots$
	11	$5d[\frac{1}{2}]_1$	9.917	10.019	$0.87(5p^55d\ ^3P_1) - 0.33(5p^55d\ ^3D_1) - 0.31(5p^56s\ ^3P_1) + 0.17(5p^56s\ ^1P_1) + \dots$
	12	$6p[\frac{1}{2}]_0$	9.934	9.867	$0.78(5p^56p\ ^1S_0) - 0.61(5p^56p\ ^3P_0) + \dots$
	13	$5d[\frac{7}{2}]_4$	9.943	10.038	$0.998(5p^55d\ ^3F_4) + \dots$
	14	$5d[\frac{3}{2}]_2$	9.959	10.065	$0.78(5p^55d\ ^3P_2) - 0.49(5p^55d\ ^3D_2) + 0.37(5p^55d\ ^1D_2) + \dots$
8	15	$5d[\frac{7}{2}]_3$	10.039	10.088	$0.76(5p^55d\ ^3F_3) + 0.60(5p^55d\ ^1F_3) - 0.23(5p^55d\ ^3D_3) + \dots$
9	16	$5d[\frac{5}{2}]_2$	10.159	10.175	$0.67(5p^55d\ ^1D_2) - 0.53(5p^55d\ ^3F_2) + 0.52(5p^55d\ ^3D_2) + \dots$
10	17	$5d[\frac{5}{2}]_3$	10.220	10.205	$0.83(5p^55d\ ^3D_3) + 0.53(5p^55d\ ^1F_3) - 0.17(5p^55d\ ^3F_3) + \dots$
11	18	$5d[\frac{3}{2}]_1$	10.401	10.394	$0.69(5p^55d\ ^1P_1) - 0.65(5p^55d\ ^3D_1) - 0.24(5p^56d\ ^1P_1) - 0.16(5p^55d\ ^3P_1) + 0.11(5p^56d\ ^3D_1) + \dots$
12	19	$7s[\frac{3}{2}]_2$	10.562	10.566	$0.99(5p^57s\ ^3P_2) + \dots$
	20	$7s[\frac{3}{2}]_1$	10.593	10.591	$0.80(5p^57s\ ^1P_1) + 0.58(5p^57s\ ^3P_1) + \dots$

Elastic DCSS for Xe have been measured by Holtkamp (1981) (5–50 eV), Register et al (1986) (1–100 eV), Nishimura et al (1987) (40–100 eV), Weyhreter et al (1988) (0.05–

Table 2. Summary of inelastic DCS measurements.

Reference	Features measured	E_0 (eV)	θ (deg)
Williams <i>et al</i> (1975)	1–11	20	0–140
Filipović <i>et al</i> (1988)	1 to 12 2 and 11	15, 20, 30 80	0–150 0–150
Nishimura <i>et al</i> (1987)	1 and 2 1 and 2 1 and 2 1	12 15 17.5 20, 25, 30, 40, 50 60, 80, 100, 120	20–120 10–125 15–125 10–120 10–125
Khakoo <i>et al</i> (1992)	r and r'	20, 30	0–134
Khakoo <i>et al</i> (1994)	r and r'	20, 30	10–120
Ester and Kessler (1994)	1 plus 2	15, 30, 40, 80, 100	6–135
Present	1 to 4	10, 15, 20, 30	0–135

2.0 eV) and by Ester and Kessler (1994) (40–100 eV). These data are in remarkably good agreement with each other.

DCSs for *electron impact excitation* of Xe are not well established. Typical energy-loss spectra, from which these cross sections can be derived, are shown in figure 1(a) and (b) at 10 and 30 eV impact energies in the 8.1–10.0 and 8.1–10.7 eV energy-loss ranges, respectively. These were obtained with our electrostatic electron energy-loss spectrometer. The experimentally resolved features in these energy-loss spectra are numbered and their assignments in terms of individual level excitations are summarized in table 1. Some features correspond to individual level excitations, others to the overlap of the excitation of two or more levels. In order to avoid confusion and to simplify the notation, we will index symbols representing scattering intensities, cross sections and their ratios by numbers corresponding to energy-loss features. Fragmentary experimental DCS data for some of these excitations are available from Williams *et al* (1975), Filipović *et al* (1988), Nishimura (1994), and Ester and Kessler (1994). The features for which the associated cross sections have been measured, the impact energies (E_0), and the scattering angle (θ) ranges for these studies are summarized in table 2. Special efforts were made recently (Khakoo *et al* 1992, 1994) to obtain accurate *ratios* for excitation cross sections associated with the four lowest features in the energy-loss spectra at 20 and 30 eV impact energies, but no cross sections were reported.

Theoretical calculations of DCSs for inelastic electron scattering by xenon were made in the past by Bartschat and Madison (1987, 1992a, b), who used the semi-relativistic distorted-wave approximation (DWA), and by Zuo *et al* (1991, 1992a), who used the relativistic DWA (RDWA).

The aims of our investigation, in general, were: (i) to establish an accurate and fairly comprehensive set of DCSs for excitation of the lowest 20 levels of Xe based on extensive measurements utilizing conventional electrostatic electron impact energy-loss spectrometers, together with a novel calibration method based on electron time-of-flight (TOF) measurements, and (ii) to calculate these DCSs using the unitarized DWA (UDWA) and unitarized first-order many-body theory (UFOMBT) with multi-configurational

wavefunctions, and assess the reliability of these methods for a large variety of processes over a wide range of impact energies (E_0) and scattering angles (θ). Measurements were carried out for the DCSs at $E_0 = 10, 15, 20$ and 30 eV in the 0 – 135° angular range. The theoretical calculations were also carried out at these energies, and in addition at 50 and 80 eV in order to compare them to the experimental results of Filipović *et al* (1988) and Nishimura (1994). The experimental procedures and theoretical methods used in our investigations, as well as results for the excitation of the lowest-lying five levels are discussed in the present paper. The accompanying paper (Khakoo *et al* 1996) describes our results for the excitation of the 6th to 20th next lowest levels.

2. Experimental methods and procedures

Three different electron energy-loss (EEL) spectrometers were used to obtain the data for this paper. Two of the instruments used electrostatic lenses and analysers to disperse the electrons according to energy with respect to space, both in the gun and the detector. These two instruments were located at California State University, Fullerton (CSUF), and Jet Propulsion Laboratory (JPL) and have been described in detail before by Khakoo *et al* (1994) and Khakoo and Trajmar (1986), respectively. We will refer to these latter instruments as electrostatic spectrometers (ES), and results obtained by them will be subscripted with ES. The third instrument used a pulsed electron gun and a field-free drift tube to disperse the energy of the scattered electrons with respect to time. It was located at JPL, and will be fully described in a forthcoming publication (LeClair *et al* 1996). We will refer to this latter instrument as the time-of-flight (TOF) spectrometer, using the subscript TOF to designate data obtained with it. Only a brief description of the three instruments will be given here.

The CSUF spectrometer used single hemispherical dispersors in the monochromator and analyser. The device was placed in a vacuum chamber, baked constantly at 120°C , and operated at background pressures ranging from 10^{-6} to 10^{-5} Torr with the gas beam on. The electron gun delivered a current of 15 – 20 nA at a resolution of about 60 meV (FWHM). The magnetic field in the chamber was reduced to below 5 mG by a mu-metal shield. The angular range covered by this apparatus was 0 to 136° . The angular resolution of the system was estimated to be $\pm 2.5^\circ$ (FWHM) and the scattering angle was measured accurately to within $\pm 1^\circ$. The incident electron energy was corrected for contact potential using the helium $1s2s^2$ Feshbach resonance at 19.36 V (Cvejanović *et al* 1974) and was found to be typically 0.38 ± 0.1 eV. The transmission of this device was tuned to be nearly constant by using the isotropic nature of the near-threshold ionization continuum of He as discussed by Nickel *et al* (1989). The target beam was formed by effusing Xe (99.9985% purity) through a capillary array. The electron beam crossed the Xe beam at a 90° angle. Energy-loss spectra (at fixed impact energies and scattering angles) were obtained by the usual pulse counting, multichannel scaling techniques. From spectra obtained with the gas beam on, the corresponding spectra obtained with the gas beam off (but same background pressure) were subtracted to eliminate background scattering.

The JPL spectrometer utilized double hemispherical energy selectors both in the electron gun and the detector. Otherwise the spectrometer and the operating conditions were similar to those described for the CSUF spectrometer. The JPL apparatus produced much cleaner energy-loss profiles (with reduced wings) and was ideal for this work where a weak energy-loss feature had to be resolved from a much stronger feature adjacent to it (e.g. feature 1 at low angles from feature 2). Typical energy resolution was about 30 meV with an electron current of 10 – 15 nA. The angular range was from 0 – 135° and the resolution was estimated at $\pm 1^\circ$ (FWHM) and the absolute scattering angle was measured accurately to within $\pm 0.5^\circ$.

The contact potential was determined by a method similar to that used for the CSUF device, and was found to be typically 0.75 ± 0.1 eV. No scans with beam off were necessary for background subtractions for this spectrometer when only inelastic features were covered in the energy-loss spectra.

EEL spectra typical to those shown in figure 1(a) and (b) were obtained by the JPL electrostatic spectrometer. The spectral features which are resolved in these spectra are numbered from 1 through 12 and in some cases represent the overlap of scattering intensities associated with excitation of more than one level. The assignment of these features in terms of level excitations is given in table 1. These spectra were fitted by our unfolding program as described previously (Khakoo *et al* 1994). The unfolding program used the energy levels (as given in table 1) and synthesized the instrumental energy-loss profile of the spectrometer using up to 5 Gaussians (or a cubic spline) and a polynomial of up to degree two for the background in the spectra. It also incorporated an algorithm which corrected deviations in our energy-loss calibrations. These spectra were used to obtain relative inelastic scattering intensities.

Lower resolution spectra, obtained with the CSUF apparatus, were unfolded in a similar way. These spectra also included the elastic peak (which we refer to as feature 0) and allowed us to extract inelastic to elastic scattering intensity ratios. In particular, the purpose of these spectra was to establish the scattering intensity ratio associated with combined features 1 and 2 and with elastic scattering at each E_0 , over the accessible angular range. These intensity ratios do not represent the inelastic to elastic DCS ratios since the instrumental response function (detection efficiency) is not the same for the two processes. Correction factors, which in the present measurements are independent of scattering angle, have to be determined at each impact energy to convert the intensity ratio curves to DCS ratio curves. Many methods to determine these correction factors have been devised, but they are complicated, inconvenient, unreliable and prone to large uncertainties, especially at electron impact energies within a few eV above the threshold of the inelastic features. We have adopted what appears to be a novel solution to this problem by constructing and using an *electron time-of-flight (TOF) spectrometer*. It was built for the purpose of obtaining TOF spectra at low impact energies. These spectra include elastic and inelastic features. The TOF spectrometer did not use any magnetostatic or electrostatic elements to collect, collimate, and disperse the scattered electrons according to their energy. Thus, evaluation of the relative intensities in a TOF spectrum requires *no energy-dependent correction factors* and the ratios of the inelastic to elastic scattering intensities are equal to the ratios of their corresponding DCSs.

Our *TOF spectrometer* used a pulsed electron gun which had an energy spread of about 0.5 eV. The pulses were approximately Gaussian in shape, and had a FWHM of about 10 ns. The electron beam intersected a gas beam, formed by a capillary tube, at right angles. A field-free drift tube was placed at $90^\circ \pm 1^\circ$ to the incident electron beam. Apertures in the drift tube defined the solid angle over which the scattered electrons were collected (apex of 6.4°). Electrons which scattered into this solid angle drifted 21.6 cm before passing a grid and encountering the post-drift accelerating field of three stacked 40 mm diameter multichannel plates. The entire apparatus was housed in a degaussed, double magnetic shield which reduced the magnetic field to 1 to 2 mG. All surfaces exposed to electrons were made from molybdenum and the entire apparatus was baked constantly at 150°C to maintain cleanliness and reduce patch fields. The vacuum chamber in which it was placed was pumped by a 25 cm oil diffusion pump, and a liquid nitrogen trap was used to reduce contamination from backstreaming.

TOF spectra were taken at impact energies ranging from 9–20 eV. Typical spectra at

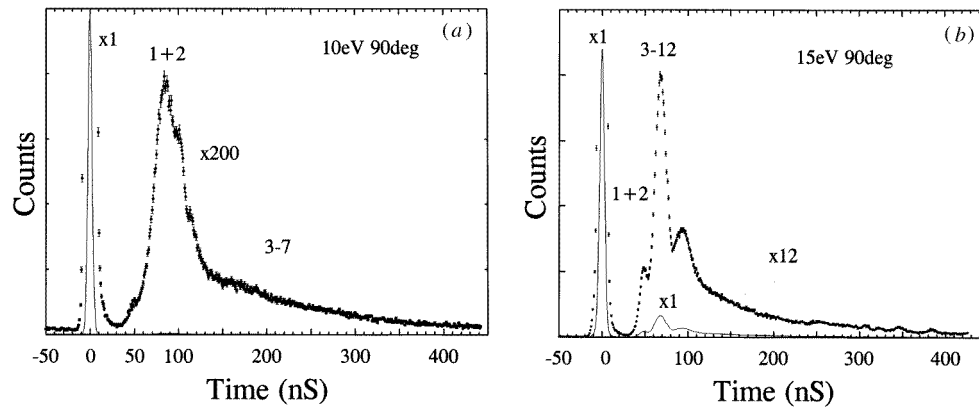


Figure 2. Time-of-flight spectra of xenon. (a) $E_0 = 10$ eV and $\theta = 90^\circ$. (b) $E_0 = 15$ eV and $\theta = 90^\circ$. Contributions from various features are indicated. The time scale was set to zero for the elastic peak.

10 and 15 eV are shown in figures 2(a) and (b), respectively. It was not possible to resolve features 1 and 2 from one another because of the energy width of the incident electron beam. Our aim here was to obtain the DCS ratios from the TOF spectra for the combined excitation represented by features 1 and 2 to that of elastic scattering. At $E_0 < 15$ eV, we would obtain this ratio directly from the TOF spectra. In order to establish the intensity of the TOF peak due to the combined features 1 and 2 at these low energies, we used the unfolding program which was described above. Here the matter was simplified since the background was always flat, and one or two Gaussians formed a sufficient fit to the peak caused by the overlap of features 1 and 2. We could not determine the intensity of the peak due to features 1 and 2 at incident energies of 15 eV and higher with any confidence.

At 15 and 20 eV impact energies we extracted from the TOF spectra the ratio of the combined scattering intensity of features 1 through 12 with respect to elastic scattering (ES) and used the ES measurements to determine the relative contribution of combined features 1 and 2 to the overall scattering intensity (including all features 1 to 12). This procedure will be discussed in more detail later. For the incident energy of 30 eV, we relied on the CSUF measurements for the scattering intensity ratio of features 1 and 2 to elastic scattering, since correction factors are insignificant for detecting scattered electrons with residual energies of 20 eV or more.

Once the intensity ratios for the combined features 1 and 2 with respect to elastic scattering were established by time of flight at the required impact energies, we used them to normalize the angular distribution curves of the same ratio measured with the electrostatic spectrometers. The result then represented the DCS ratios of the combined features 1 and 2 with respect to elastic scattering. Utilizing these DCS ratios and the elastic DCSs of Register *et al* (1986), we obtained DCSs for the combined features 1 and 2 at various energies, which in turn served as secondary standards for normalizing all other inelastic DCSs.

3. Experimental results

Energy-loss spectra, including the elastic peak and the 8.1 to 10.7 eV energy-loss region, were taken at 10, 15, 20 and 30 eV impact energies in the 0 – 135° angular range with the

Table 3. Summary of the intensity ratios at $\theta = 90^\circ$ which are pertinent to the absolute calibrations.

E_0 (eV)	Time of flight		Energy loss		TOF and E loss R_0^{1+2}
	R_0^{1+2}	R_0^{1-12}	R_{1-12}^{1+2}	R_0^{1+2}	
9	0.020 ± 0.002	—	—	—	—
10	0.027 ± 0.003	—	—	—	—
11	0.030 ± 0.002	—	—	—	—
15	—	0.212 ± 0.007	0.126 ± 0.014	—	0.027 ± 0.003
20	—	0.208 ± 0.015	0.127 ± 0.014	—	0.026 ± 0.003
30	—	—	0.175 ± 0.019	0.037 ± 0.002	—

Table 4. Summary of present R_0^{1+2} , r , r' , r'' , and DCS values for the various energy-loss features at $E_0 = 10$ eV. The R_0^{1+2} values correspond to the smooth curve drawn through the experimental points obtained in the ES measurements and then normalized at 90° to the time-of-flight value. The numbers at the top of the DCS columns refer to feature numbers (see table 1). The units for the DCSs are $\text{cm}^2 \text{sr}^{-1}$ (the exponent to which 10 should be raised to get the proper multiplying factor for each case is indicated).

Scattering angle (deg)	R_0^{1+2}									
		r	r'	r''	(1 + 2)	1	2	3	4	
20	0.0019	31.4	9.6	0.72	4.37E-18	1.82E-18	2.55E-18	5.81E-20	2.7E-19	
25	0.0022	24.2	9.3	0.73	3.81E-18	1.6E-18	2.2E-18	6.63E-20	2.4E-19	
30	0.0022	21.7	8.9	0.74	2.97E-18	1.26E-18	1.71E-18	5.79E-20	1.9E-19	
35	0.0026	21.2	8.5	0.74	2.6E-18	1.1E-18	1.49E-18	5.19E-20	1.8E-19	
40	0.0030	22.7	8.0	0.73	2.21E-18	9.34E-19	1.28E-18	4.11E-20	1.6E-19	
45	0.0041	24.6	7.4	0.71	2.07E-18	8.63E-19	1.21E-18	3.5E-20	1.6E-19	
50	0.0053	24.5	6.9	0.68	1.97E-18	8.01E-19	1.17E-18	3.27E-20	1.7E-19	
60	0.010	17.5	5.9	0.61	1.91E-18	7.26E-19	1.19E-18	4.15E-20	2E-19	
70	0.016	12.7	5.7	0.56	1.8E-18	6.46E-19	1.15E-18	5.07E-20	2E-19	
80	0.020	12.1	5.8	0.55	1.78E-18	6.32E-19	1.15E-18	5.21E-20	2E-19	
90	0.027	14.1	7.7	0.58	1.94E-18	7.12E-19	1.23E-18	5.06E-20	1.6E-19	
95	0.032	16.5	9.1	0.60	2.1E-18	7.9E-19	1.31E-18	4.78E-20	1.5E-19	
100	0.039	19.2	10.6	0.62	2.29E-18	8.8E-19	1.41E-18	4.58E-20	1.3E-19	
110	0.069	24.4	11.5	0.65	3.3E-18	1.3E-18	2E-18	5.31E-20	1.7E-19	
120	0.099	24.4	9.6	0.61	4.73E-18	1.79E-18	2.94E-18	7.33E-20	3.1E-19	
130	0.082	19.6	7.2	0.52	5.84E-18	1.99E-18	3.85E-18	1.02E-19	5.3E-19	
135	0.071	17.2	6.1	0.46	6.49E-18	2.06E-18	4.43E-18	1.19E-19	7.3E-19	
Error %	11.3	10.0	11.3	7.1	12.4	18	13	19.1	15.9	

electrostatic spectrometers. From these ES spectra, we deduced a number of scattering intensity ratios which are defined as:

$$R_0^{1+2}(E_0, \theta)_{\text{ES}} \equiv \frac{I_{1+2}(E_0, \theta)_{\text{ES}}}{I_0(E_0, \theta)_{\text{ES}}} \quad (1)$$

$$R_{1+2}^3(E_0, \theta)_{\text{ES}} \equiv \frac{I_3(E_0, \theta)_{\text{ES}}}{I_{1+2}(E_0, \theta)_{\text{ES}}} = \frac{DCS_3(E_0, \theta)}{DCS_{1+2}(E_0, \theta)} \equiv R_{1+2}^3(E_0, \theta) \quad (2)$$

Table 5. Same as table 4, except for $E_0 = 15$ eV. Here the ES experimental values of R_0^{1+2} also include those derived from the data of Ester and Kessler (1994), Nishimura *et al* (1987) and Filipović *et al* (1988).

Scattering angle (deg)	R_0^{1+2}	r	r'	r''	(1 + 2)	1	2	3	4
0	0.0044	2.82	3.09	0.105	2.48E-17	2.35E-18	2.24E-17	8.34E-19	7.25E-18
3	0.0035	2.28	3.11	0.084	1.88E-17	1.46E-18	1.73E-17	6.39E-19	5.58E-18
5	0.0034	2.20	3.08	0.082	1.71E-17	1.3E-18	1.58E-17	5.9E-19	5.13E-18
6	0.0032				1.58E-17				
8	0.0032	1.99	3.03	0.085	1.48E-17	1.16E-18	1.36E-17	5.81E-19	4.49E-18
10	0.0030	1.83	2.92	0.088	1.27E-17	1.03E-18	1.17E-17	5.63E-19	4.01E-18
12	0.0027	1.75		0.095	1.09E-17	9.48E-19	9.98E-18	5.43E-19	3.54E-18
15	0.0023	1.60	2.56	0.115	8.08E-18	8.33E-19	7.24E-18	5.2E-19	2.83E-18
20	0.0025	1.80	1.86	0.18	6.6E-18	1.01E-18	5.6E-18	5.59E-19	3.01E-18
25	0.0025	2.08	1.71	0.245	4.91E-18	9.67E-19	3.95E-18	4.64E-19	2.31E-18
30	0.0029	2.43	1.73	0.296	3.94E-18	9E-19	3.04E-18	3.71E-19	1.75E-18
35	0.0040	2.72	1.73	0.293	3.57E-18	8.08E-19	2.76E-18	2.97E-19	1.59E-18
40	0.0063	3.01	1.75	0.265	3.58E-18	7.49E-19	2.83E-18	2.49E-19	1.62E-18
45	0.0097	2.83	1.71	0.227	3.22E-18	5.96E-19	2.63E-18	2.11E-19	1.54E-18
50	0.016	2.64	1.59	0.198	3.17E-18	5.24E-19	2.65E-18	1.98E-19	1.66E-18
55	0.023				2.83E-18				
60	0.032	1.82	1.25	0.153	2.79E-18	3.71E-19	2.42E-18	2.04E-19	1.93E-18
65	0.032				2.26E-18				
70	0.033	1.34	1.01	0.164	2.17E-18	3.06E-19	1.87E-18	2.28E-19	1.84E-18
75	0.029				1.77E-18				
80	0.029	1.46	0.84	0.287	1.6E-18	3.57E-19	1.24E-18	2.45E-19	1.48E-18
85	0.026				1.27E-18				
90	0.027	1.51	0.90	0.335	1.14E-18	2.87E-19	8.56E-19	1.9E-19	9.49E-19
95	0.032	1.55	0.94	0.34	1.22E-18	3.1E-19	9.1E-19	2E-19	9.7E-19
100	0.032	1.59	0.92	0.34	1.23E-18	3.11E-19	9.15E-19	1.96E-19	9.93E-19
105	0.031				1.24E-18				
110	0.030	1.76	0.73	0.372	1.38E-18	3.74E-19	1.01E-18	2.12E-19	1.38E-18
115	0.028				1.43E-18				
120	0.027	1.96	0.57	0.491	1.49E-18	4.9E-19	9.97E-19	2.5E-19	1.74E-18
125	0.028				1.56E-18				
130	0.026	2.11	0.53	0.594	1.4E-18	5.22E-19	8.79E-19	2.48E-19	1.65E-18
135	0.025	2.41	0.50	0.783	1.23E-18	5.4E-19	6.9E-19	2.24E-19	1.38E-18
140					1.12E-18				
Error %	13.0		7.5	11.3	10.2	19.1	12.8	16.2	15.4

$$R_{1+2}^4(E_0, \theta)_{\text{ES}} \equiv \frac{I_4(E_0, \theta)_{\text{ES}}}{I_{1+2}(E_0, \theta)_{\text{ES}}} = \frac{DCS_4(E_0, \theta)}{DCS_{1+2}(E_0, \theta)} \equiv R_{1+2}^4(E_0, \theta) \quad (3)$$

$$R_{1 \text{ to } 12}^{1+2}(E_0, \theta)_{\text{ES}} \equiv \frac{I_{1+2}(E_0, \theta)_{\text{ES}}}{I_{1 \text{ to } 12}(E_0, \theta)_{\text{ES}}} = \frac{DCS_{1+2}(E_0, \theta)}{DCS_{1 \text{ to } 12}(E_0, \theta)} \equiv R_{1 \text{ to } 12}^{1+2}(E_0, \theta) \quad (4)$$

$$r(E_0, \theta)_{\text{ES}} \equiv \frac{I_1(E_0, \theta)_{\text{ES}}}{I_3(E_0, \theta)_{\text{ES}}} = \frac{DCS_1(E_0, \theta)}{DCS_3(E_0, \theta)} \equiv r(E_0, \theta) \quad (5)$$

$$r'(E_0, \theta)_{\text{ES}} \equiv \frac{I_2(E_0, \theta)_{\text{ES}}}{I_4(E_0, \theta)_{\text{ES}}} = \frac{DCS_2(E_0, \theta)}{DCS_4(E_0, \theta)} \equiv r'(E_0, \theta) \quad (6)$$

Table 6. Same as table 4, but for $E_0 = 20$ eV. Here the ES experimental values of R_0^{1+2} also include those derived from the data of Nishimura *et al* (1987) and Filipović *et al* (1988).

Scattering angle (deg)	R_0^{1+2}	r	r'	r''	(1 + 2)	1	2	3	4
0	0.029	1.80	2.76	0.017	1.94E-16	3.24E-18	1.91E-16	1.8E-18	6.9E-17
3	0.017	1.81	2.66	0.020	9.49E-17	1.89E-18	9.3E-17	1.04E-18	3.49E-17
5	0.013	1.95	2.60	0.025	6.79E-17	1.66E-18	6.62E-17	8.49E-19	2.55E-17
8	0.011	2.17	2.45	0.035	4.92E-17	1.66E-18	4.76E-17	7.63E-19	1.94E-17
10	0.010	2.12	2.33	0.040	4.14E-17	1.58E-18	3.98E-17	7.45E-19	1.71E-17
12	0.009	2.01	2.23	0.044	3.30E-17	1.39E-18	3.16E-17	6.93E-19	1.42E-17
15	0.007	2.05	1.99	0.061	2.28E-17	1.31E-18	2.15E-17	6.38E-19	1.08E-17
20	0.007	1.93	1.75	0.085	1.58E-17	1.24E-18	1.45E-17	6.41E-19	8.3E-18
25	0.008	1.99	1.63	0.110	1.31E-17	1.3E-18	1.18E-17	6.52E-19	7.24E-18
30	0.008	1.86	1.54	0.120	8.59E-18	9.2E-19	7.67E-18	4.94E-19	4.96E-18
35	0.011	1.77	1.52	0.118	7.12E-18	7.51E-19	6.37E-18	4.24E-19	4.2E-18
40	0.016	1.65	1.49	0.112	4.85E-18	4.88E-19	4.36E-18	2.96E-19	2.92E-18
45	0.032	1.66	1.46	0.115	3.85E-18	3.97E-19	3.45E-18	2.39E-19	2.37E-18
50	0.093	1.75	1.40	0.122	3.26E-18	3.55E-19	2.91E-18	2.03E-19	2.07E-18
60	0.112	2.10	1.27	0.154	2.91E-18	3.88E-19	2.52E-18	1.85E-19	1.99E-18
70	0.030	2.26	1.11	0.173	1.92E-18	2.84E-19	1.64E-18	1.25E-19	1.47E-18
80	0.017	1.90	1.01	0.171	9.79E-19	1.43E-19	8.36E-19	7.54E-20	8.29E-19
90	0.026	1.38	0.95	0.170	6.85E-19	9.95E-20	5.85E-19	7.19E-20	6.16E-19
95	0.046	1.17	0.91	0.174	6.94E-19	1.03E-19	5.91E-19	8.81E-20	6.46E-19
100	0.133	1.13	0.85	0.197	6.66E-19	1.1E-19	5.56E-19	9.72E-20	6.55E-19
110	0.073	1.37	0.77	0.275	6.54E-19	1.41E-19	5.13E-19	1.03E-19	6.67E-19
120	0.034	2.08	0.74	0.402	5.90E-19	1.69E-19	4.21E-19	8.14E-20	5.71E-19
130	0.036	3.11	0.86	0.477	5.82E-19	1.88E-19	3.94E-19	6.05E-20	4.58E-19
135	0.066	4.30	1.00	0.467	7.23E-19	2.3E-19	4.93E-19	5.35E-20	4.92E-19
140									
Error %	10.3	7.7	7.2	11.3	7.2	14.2	11.2	15.6	13.6

$$r''(E_0, \theta)_{\text{ES}} \equiv \frac{I_1(E_0, \theta)_{\text{ES}}}{I_2(E_0, \theta)_{\text{ES}}} = \frac{DCS_1(E_0, \theta)}{DCS_2(E_0, \theta)} \equiv r''(E_0, \theta). \quad (7)$$

$I_N(E_0, \theta)_{\text{ES}}$ refers to the scattering intensity of feature N measured by the electrostatic instrument for impact energy E_0 and electron scattering angle θ . The superscripted and subscripted index numbers refer to the *feature numbers* listed in table 1. The index 0 refers to the elastic scattering feature. The indices 1 + 2 and 1 to 12 refer to combined 1 and 2 and 1 through 12 features, respectively. The ratios defined by equations (2)–(6) are required for the derivation of the absolute inelastic DCSs (DCS_N s where $N = 1, 2, 3,$ and 4). Equations (5) and (6) are defined in accordance with Khakoo *et al* (1994) and are also used to check whether the statistical weight ratios represent the DCS ratios for the predominantly $J = 2$ and 0 levels ($6s[\frac{3}{2}]_2$ and $6s'[\frac{1}{2}]_0$) and to establish the DCS ratios associated with features 2 and 4 ($6s[\frac{3}{2}]_1$, and $6s'[\frac{1}{2}]_1$ and $6p[\frac{1}{2}]_1$, respectively). Equation (7) is used for checking purposes.

The ratio defined in equation (1) does not, in general, represent the corresponding DCS ratio, as do the other ratios in equations (2)–(7). This is because the instrument response function, $F(E_0)$, may depend on the residual energy (E_r) of the scattered electrons at residual energies less than about 20 eV. Thus, the actual DCS ratio associated with the combined features 1 and 2 and the elastic feature must be related to the corresponding ES

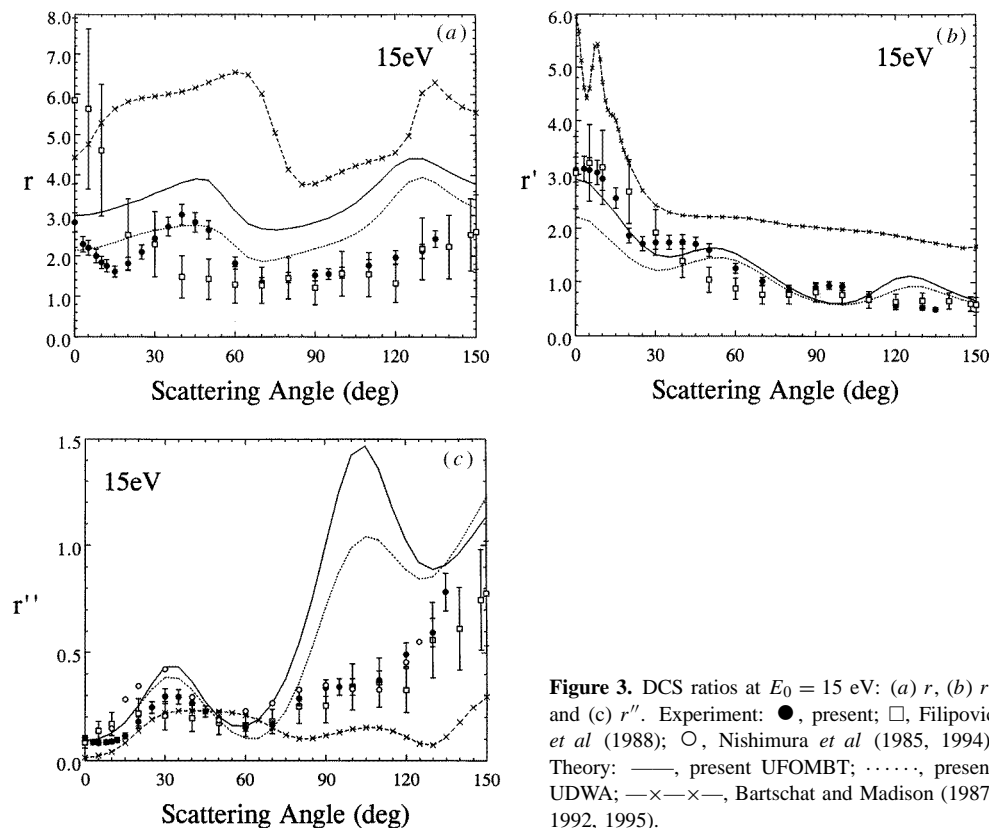


Figure 3. DCS ratios at $E_0 = 15$ eV: (a) r , (b) r' and (c) r'' . Experiment: \bullet , present; \square , Filipović *et al* (1988); \circ , Nishimura *et al* (1985, 1994). Theory: —, present UFOMBT; \cdots , present UDWA; $-\times-\times-$, Bartschat and Madison (1987, 1992, 1995).

intensity ratio by

$$R_0^{1+2}(E_0, \theta) \equiv \frac{DCS_{1+2}(E_0, \theta)}{DCS_0(E_0, \theta)} = R_0^{1+2}(E_0, \theta)_{ES} F(E_0). \quad (8)$$

At $E_0 \geq 30$ eV, $F(E_0)$ is approximately unity.

From the TOF spectra, we derived the following ratios:

$$R_0^{1+2}(E_0, 90^\circ)_{TOF} \equiv \frac{I_{1+2}(E_0, 90^\circ)_{TOF}}{I_0(E_0, 90^\circ)_{TOF}} = \frac{DCS_{1+2}(E_0, 90^\circ)}{DCS_0(E_0, 90^\circ)} \equiv R_0^{1+2}(E_0, 90^\circ) \quad (9)$$

$$R_0^{1 \text{ to } 12}(E_0, 90^\circ)_{TOF} \equiv \frac{I_{1 \text{ to } 12}(E_0, 90^\circ)_{TOF}}{I_0(E_0, 90^\circ)_{TOF}} = \frac{DCS_{1 \text{ to } 12}(E_0, 90^\circ)}{DCS_0(E_0, 90^\circ)} \equiv R_0^{1 \text{ to } 12}(E_0, 90^\circ). \quad (10)$$

The measurements were performed in seven steps.

(i) The $R_0^{1+2}(E_0, 90^\circ)$ values were established. At $E_0 < 15$ eV this was achieved directly from the TOF spectra using equation (9). At $E_0 = 15$ and 20 eV, we utilized equations (10) and (4) and obtained $R_0^{1+2}(E_0, 90^\circ) = R_0^{1 \text{ to } 12}(E_0, 90^\circ) R_{1 \text{ to } 12}^{1+2}(E_0, 90^\circ)_{ES}$. At $E_0 = 30$ eV we used equation (1) and assumed that $R_0^{1+2}(E_0, \theta)_{ES} = R_0^{1+2}(E_0, \theta)$. The ratios pertinent to this step are listed in table 3.

(ii) The $R_0^{1+2}(E_0, \theta)_{ES}$ ratios were normalized to $R_0^{1+2}(E_0, 90^\circ)$ to get $R_0^{1+2}(E_0, \theta)$. This amounted to obtaining $F(E_0)$ in equation (8). We also normalized the $R_0^{1+2}(E_0, \theta)_{ES}$ ratios obtained from the measurements of Nishimura *et al* (1985), Filipović *et al* (1988) and Ester and Kessler (1994), where available, to our TOF results and plotted them together

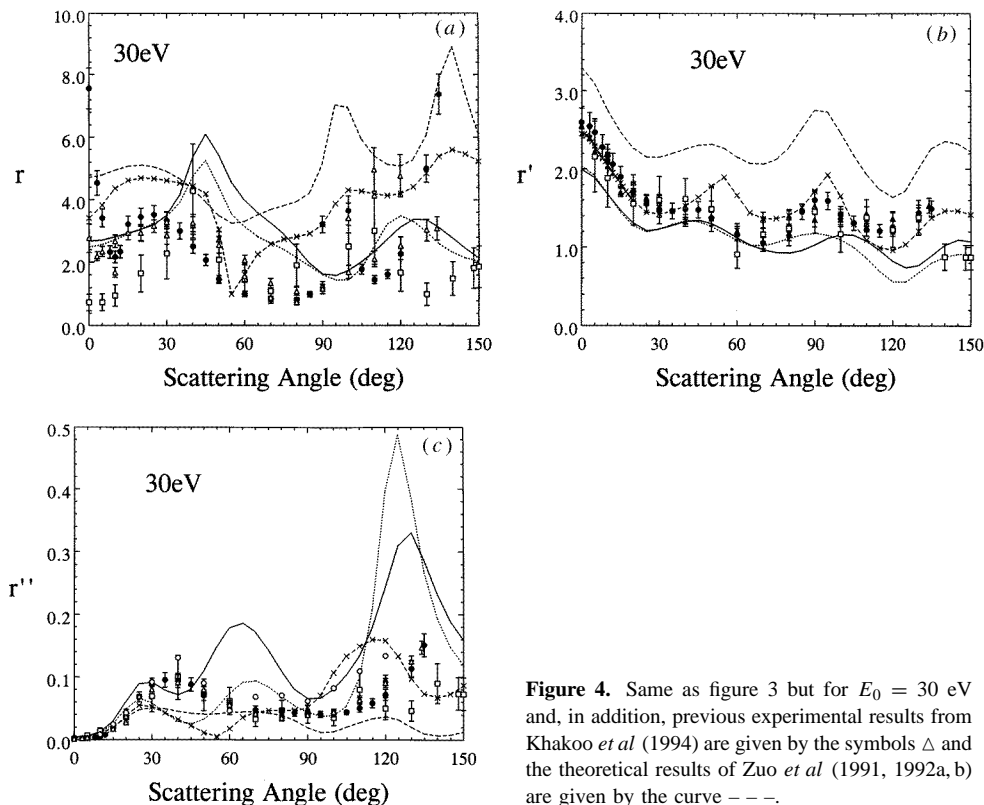


Figure 4. Same as figure 3 but for $E_0 = 30$ eV and, in addition, previous experimental results from Khakoo *et al* (1994) are given by the symbols Δ and the theoretical results of Zuo *et al* (1991, 1992a, b) are given by the curve ---.

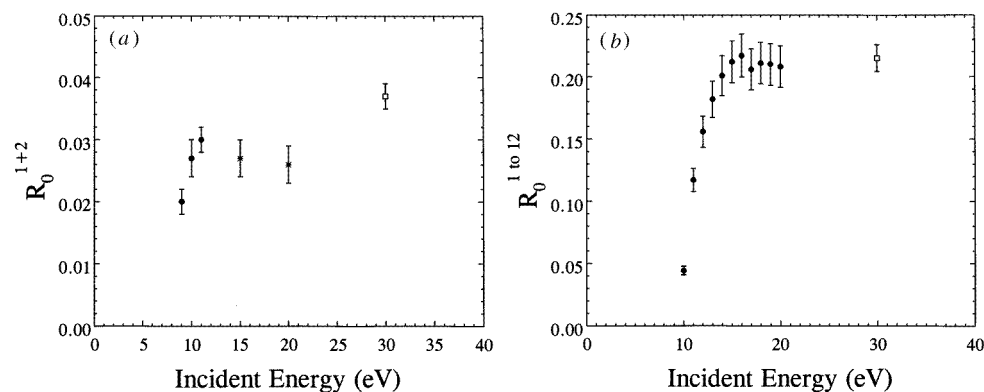


Figure 5. DCS ratios at $\theta = 90^\circ$: (a) R_0^{1+2} and (b) $R_0^{1 \text{ to } 12}$. The symbols \bullet , \square and $*$ refer to values obtained from TOF, ES and combined TOF and ES measurements, respectively.

with the present values. A smooth curve was then drawn through all points and the values corresponding to this smooth curve were used in step (iii).

(iii) From $R_0^{1+2}(E_0, \theta)$ and $\text{DCS}_0(E_0, \theta)$ of Register *et al* (1986) we derived $\text{DCS}_{1+2}(E_0, \theta)$. At small θ , the elastic phase shift data of Register *et al* (1986) were utilized to extrapolate these quantities to zero angle.

(iv) The R_{1+2}^3 and R_{1+2}^4 ratio data were fitted to a smooth curve at each E_0 as a function

Table 7. Same as table 4, but for $E_0 = 30$ eV. Here the ES experimental values of R_0^{1+2} also include those derived from the data of Ester and Kessler (1994) and Nishimura *et al* (1987).

Scattering angle (deg)	R_0^{1+2}	r	r'	r''	(1 + 2)	1	2	3	4
0	0.0863	7.56	2.60	0.0025	2.4E-16	5.99E-19	2.39E-16	7.92E-20	9.22E-17
3	0.0777	4.54	2.55	0.0021	2.05E-16	4.38E-19	2.05E-16	9.64E-20	8.04E-17
5	0.0718	3.41	2.47	0.0024	1.78E-16	4.19E-19	1.78E-16	1.23E-19	7.19E-17
6	0.0670				1.61E-16				
8	0.0537	2.33	2.28	0.0035	1.15E-16	4.02E-19	1.15E-16	1.73E-19	5.04E-17
10	0.0384	2.17	2.16	0.0049	7.53E-17	3.68E-19	7.49E-17	1.69E-19	3.45E-17
12	0.0313	2.33	2.06	0.0080	5.32E-17	4.22E-19	5.28E-17	1.81E-19	2.56E-17
15	0.0245	3.20	1.90	0.018	3.36E-17	6.03E-19	3.3E-17	1.88E-19	1.74E-17
20	0.0158	3.44	1.71	0.043	1.42E-17	5.86E-19	1.36E-17	1.7E-19	7.97E-18
25	0.0148	3.52	1.55	0.068	8.54E-18	5.44E-19	8E-18	1.55E-19	5.16E-18
30	0.0164	3.33	1.48	0.087	5.54E-18	4.43E-19	5.1E-18	1.33E-19	3.43E-18
35	0.0210	2.99	1.46	0.095	3.96E-18	3.45E-19	3.63E-18	1.15E-19	2.49E-18
40	0.0292	2.50	1.48	0.094	2.6E-18	2.23E-19	2.37E-18	8.93E-20	1.6E-18
45	0.0546	2.07	1.48	0.088	2.03E-18	1.63E-19	1.86E-18	7.89E-20	1.26E-18
50	0.0925	1.46	1.37	0.070	1.41E-18	9.25E-20	1.31E-18	6.33E-20	9.57E-19
60	0.0402	1.00	1.16	0.056	9.6E-19	5.09E-20	9.09E-19	5.09E-20	7.86E-19
70	0.0192	0.84	1.05	0.048	7.14E-19	3.27E-20	6.81E-19	3.9E-20	6.47E-19
80	0.0186	0.82	1.21	0.044	5.16E-19	2.19E-20	4.94E-19	2.69E-20	4.08E-19
85	0.0236	0.99	1.45	0.043	4.67E-19	1.93E-20	4.47E-19	1.95E-20	3.08E-19
90	0.0374	3.20	1.60	0.042	4.96E-19	1.99E-20	4.78E-19	6.22E-21	2.98E-19
95	0.0460	13.42	1.59	0.041	5.15E-19	2E-20	4.95E-19	1.49E-21	3.11E-19
100	0.0334	3.65	1.42	0.042	4.84E-19	1.94E-20	4.65E-19	5.33E-21	3.27E-19
105	0.0194	1.78	1.31	0.044	4.12E-19	1.72E-20	3.94E-19	9.67E-21	3.01E-19
110	0.0122	1.45	1.23	0.051	3.62E-19	1.74E-20	3.45E-19	1.2E-20	2.81E-19
115	0.0084	1.62	1.21	0.058	2.86E-19	1.57E-20	2.7E-19	9.71E-21	2.23E-19
120	0.0082	2.27	1.26	0.072	2.72E-19	1.82E-20	2.54E-19	7.99E-21	2.02E-19
125	0.0102				2.74E-19				
130	0.0185	5.00	1.44	0.113	3.2E-19	3.25E-20	2.87E-19	6.5E-21	2E-19
135	0.0519	7.37	1.49	0.151	3.84E-19	5.04E-20	3.34E-19	6.83E-21	2.24E-19
140					3.9E-19				
Error %	5.6	10.0	6.9	11.9	10.6	14.3	11.2	16.6	12.3

Table 8. Summary of experimental errors.

Energy (eV)	Sources of error (%)					Total (%)
	Elastic to inelastic ratio	Elastic DCSs	Spectrum unfolding	Statistical		
10	3	5	1.5-15	1-1.5	6-22	
15	3	5	2-18	1-20	6-28	
20	3	6	2-17	2-13	7-23	
30	3	9	2-16	1-15	10-25	

of θ . Then from the $R_{1+2}^3(E_0, \theta)$ and $R_{1+2}^4(E_0, \theta)$ values (obtained from the smooth curves), and from $DCS_{1+2}(E_0, \theta)$, we obtained $DCS_3(E_0, \theta)$ and $DCS_4(E_0, \theta)$.

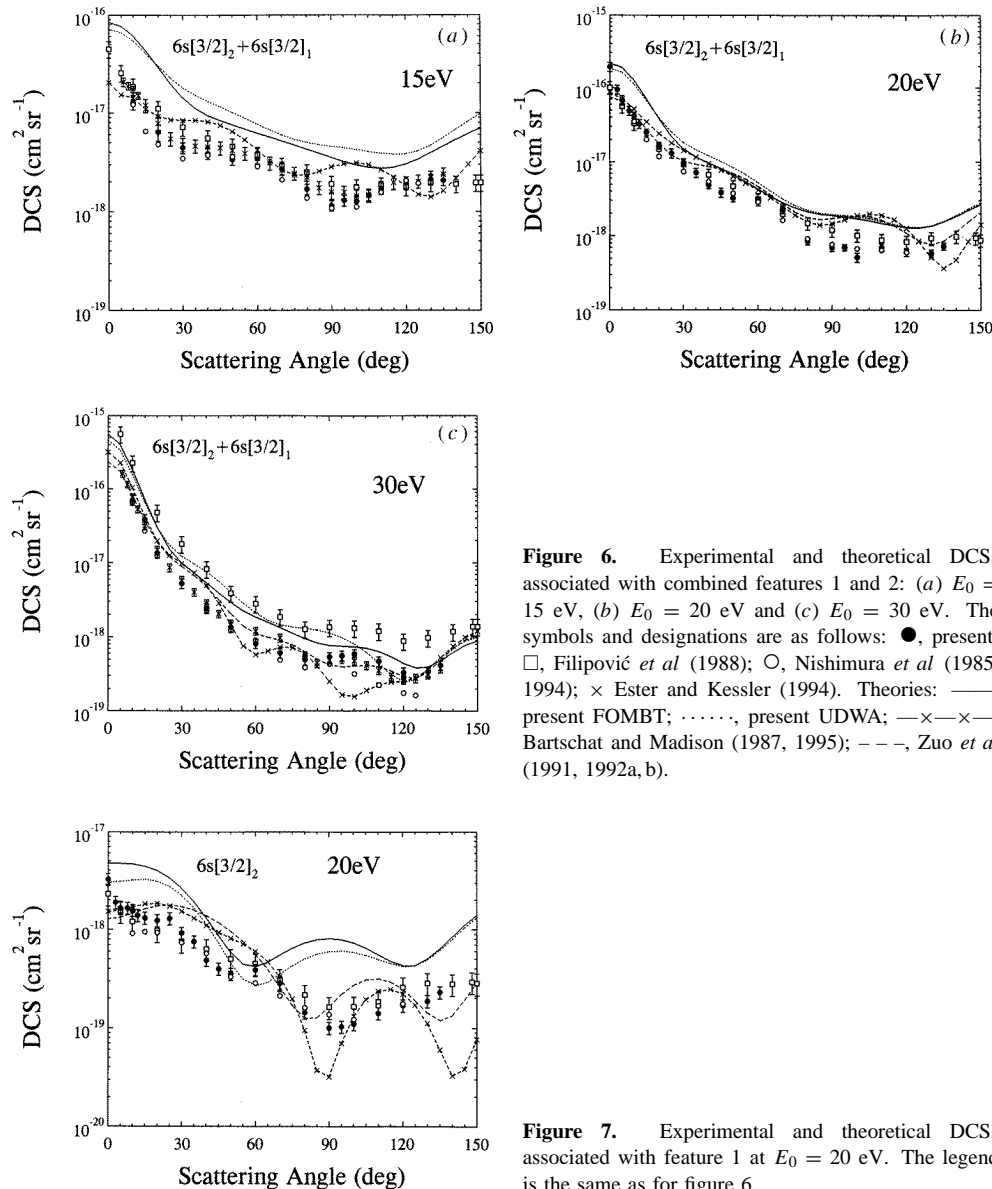


Figure 6. Experimental and theoretical DCSs associated with combined features 1 and 2: (a) $E_0 = 15$ eV, (b) $E_0 = 20$ eV and (c) $E_0 = 30$ eV. The symbols and designations are as follows: ●, present; □, Filipović *et al* (1988); ○, Nishimura *et al* (1985, 1994); × Ester and Kessler (1994). Theories: —, present FOMBT; ·····, present UDWA; —×—×—, Bartschat and Madison (1987, 1995); ---, Zuo *et al* (1991, 1992a, b).

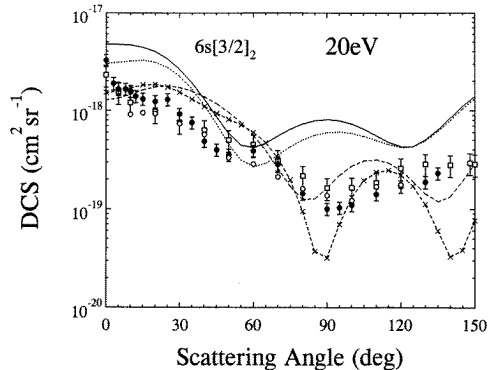


Figure 7. Experimental and theoretical DCSs associated with feature 1 at $E_0 = 20$ eV. The legend is the same as for figure 6.

(v) The r data were fitted to a smooth curve at each E_0 as a function of θ . Then from the $r(E_0, \theta)$ values (obtained from the smooth curves) and from $DCS_3(E_0, \theta)$, we obtained $DCS_1(E_0, \theta)$.

(vi) The r' data were fitted to a smooth curve at each E_0 as a function of θ . Then from the $r'(E_0, \theta)$ values (obtained from the smooth curves) and from $DCS_4(E_0, \theta)$ we obtained $DCS_2(E_0, \theta)$.

(vii) The $r''(E_0, \theta)$ values were checked.

The present experimental ratios $r(E_0, \theta)$, $r'(E_0, \theta)$, $r''(E_0, \theta)$ and $R_0^{1+2}(E_0, \theta)$ and the $DCS_n(E_0, \theta)$ ($n = 1, 2, 3$ and 4) values are summarized in tables 4–7. Table 8 contains a summary of errors. Representative comparisons between present experimental

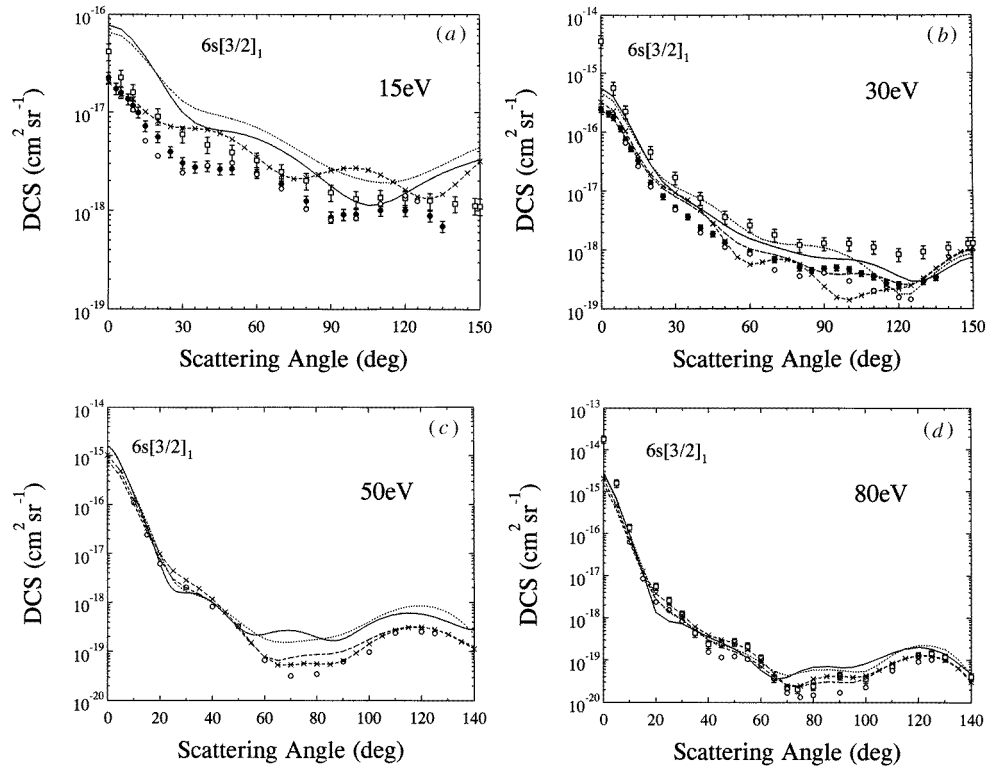


Figure 8. Experimental and theoretical DCSs associated with feature 2: (a) $E_0 = 15$ eV, (b) $E_0 = 30$ eV, (c) $E_0 = 50$ eV, (d) $E_0 = 80$ eV. The legend is the same as for figure 6.

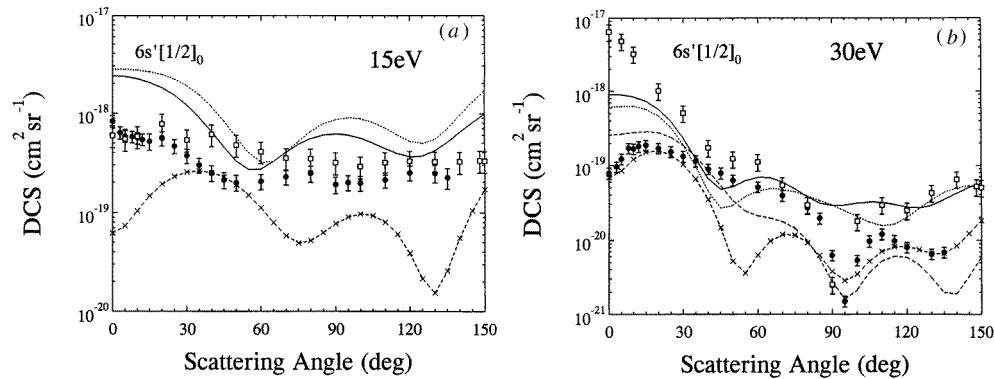


Figure 9. Experimental and theoretical DCSs associated with feature 3: (a) $E_0 = 15$ eV and (b) $E_0 = 30$ eV. The legend is the same as for figure 6.

and theoretical results and with earlier experimental and theoretical results are shown in figures 3–10. A full set of figures comparing all available experimental results with those from theoretical calculations can be found in a Los Alamos National Laboratory Report (Fontes *et al* 1996).

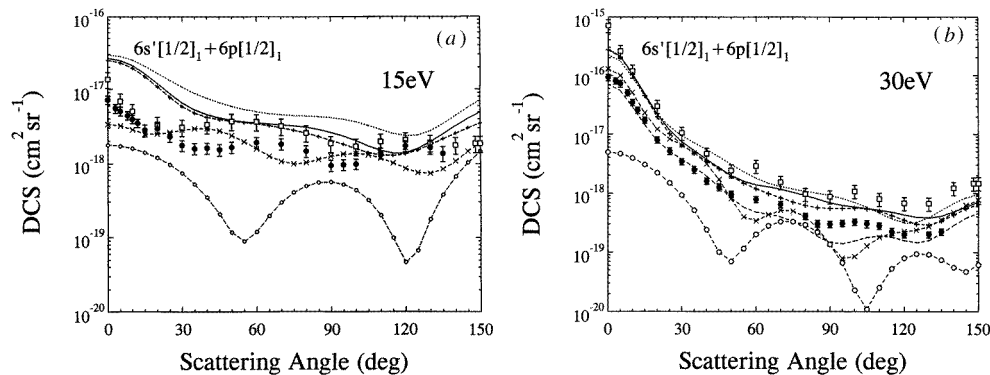


Figure 10. Experimental and theoretical DCSs associated with feature 4: (a) $E_0 = 15$ eV and (b) $E_0 = 30$ eV. The legend is the same as for figure 6 but, in addition, the DCSs for the two levels associated with this feature are also shown individually as obtained from the UFOMBT calculation. $-+--+$ and $-o-o-$ represent DCSs for excitation of levels 4 and 5 respectively. For our UDWA calculation only the sum is given. For the calculations of Bartschat and Madison (1987, 1995) and Zuo *et al* (1991, 1992a, b) only the dominant, level 4 DCS was considered.

4. Theory and calculational methods

The method of calculation was described earlier in detail by Clark *et al* (1989, 1991) and will be only briefly summarized here. The calculations were performed by the subsequent running of three computer codes named CATS, ACE and TAPS. Atomic structure calculations were performed with the CATS code (Abdallah *et al* 1988), a modified version of Cowan's atomic structure codes (Cowan 1968a, b, 1981, Cowan and Griffin 1967). The atomic structure calculation is initiated by a single configuration Hartree-Fock calculation for the radial wavefunctions of each configuration. Mixing among all configurations and LS terms with the same total angular momentum J and parity is then obtained through diagonalizing the Hamiltonian on the given basis set.

The electron collision calculations were performed using the ACE code (Clark *et al* 1988a). This code reads in data from the atomic structure file and calculates electron-impact-excitation radial integrals and angular factors using a variety of options. The ACE code uses the DWA of Mann (1983) or the FOMBT of Csanak *et al* (1971). The only difference between the DWA and FOMBT calculations is that in the former case (i.e. for DWA), we calculate the continuum wavefunctions in the potential of the initial and final configurations for the incident and scattered electrons, respectively, whereas in the latter case (i.e. for FOMBT), the same potential (that of the initial configuration) is used for both continuum electrons. The reactance matrix elements are first calculated between LS terms. Unitarization of the reactance matrix is normally carried out providing the UDWA and UFOMBT results (however, unitarization can be ignored for comparison purposes). Recoupling is then done using the pair-coupling scheme of Saraph (1972). Inclusion of the configuration-interaction and intermediate-coupling mixing is obtained as by Clark (1978).

If desired, the user can request DCSs from the ACE code. The ACE code then uses the reactance matrix along with continuum wavefunction phases to calculate the scattering amplitudes using the recoupling scheme of Inal and Dubau (1987). The scattering amplitudes are stored on a data file and can be used to calculate DCSs via the TAPS code (Clark *et al* 1988b). For the present calculations a 12 configuration basis set was used which resulted

in 77 levels. The chosen basis set ensured that all important configuration mixing was included for the calculation of the wavefunctions associated with the ground and lowest 20 excited levels for xenon. It is these 21 levels that are involved in the 12 experimentally measured features discussed in the present and accompanying paper (see table 1). Table 1 lists the dominant LSJ terms for these lowest-lying levels. All theoretical cross sections were calculated with 100 partial waves for the continuum electron to ensure numerical convergence.

5. Results and discussion

5.1. Intensity and DCS ratios

The measured scattering intensities and the corresponding DCS ratios are defined by equations (1)–(10).

In an earlier communication, Khakoo *et al* (1994) reported r and r' values at 20 and 30 eV impact energies. Here we report results from additional measurements at these energies and from extension of these measurements to 10 and 15 eV impact energies. These intensity ratios represent the corresponding DCS ratios since instrumental effects over a small energy-loss range can be considered nearly constant. The r values are related to features 1 and 3 (i.e. excitation of levels 1 and 3 which are predominantly 3P_2 and 3P_0 , respectively). These ratios show large deviations from the statistical weight ratio of five, and from theoretically obtained values, especially as the impact energy decreases. There are considerable disagreements between the present and earlier experimental results at some angles at all impact energies. Typical r values are shown at $E_0 = 15$ and 30 eV in figures 3(a) and 4(a), respectively. The deviation of the semirelativistic results of Bartschat and Madison (1995) from the statistical value of five is due to the slightly different threshold energies of the two levels and the incorporation of semirelativistic (e.g. spin-orbit coupling) effects into the calculation of the continuum orbitals. The strong deviation of the UFOMBT and UDWA results from five is due to the fact that the wavefunctions used in these calculations incorporate a strong contribution (with a coefficient of 0.41) of the $5p^55d$ configuration to the 3P_0 term, while the 3P_2 wavefunction almost exclusively comes from the $5p^56s$ configuration. The deviation of the present UFOMBT and UDWA results from those of Khakoo *et al* (1994) at $E_0 = 30$ eV is due to the fact that the earlier calculation did not include the $5p^55d$ configuration in the basis set. The r' values relate to the $6s[\frac{3}{2}]_1$ level and to the combined $6s[\frac{1}{2}]_1$ and $6p[\frac{1}{2}]_1$ unresolved level excitations. The first two levels are predominantly mixtures of 3P_1 and 1P_1 terms, while the third level is mainly a 3S_1 , 3P_1 and 1P_1 combination (see table 1). These ratios can be accurately measured and serve to more rigorously check the calculational schemes. The present experimental ratios and those reported by Khakoo *et al* (1994) agree well with each other but the rather large disagreement at certain angles and energies with the ratios obtained by Filipović *et al* (1988) is puzzling. None of the theoretical results agree with experiment at all energies. The closest overall agreement is found for the UFOMBT calculations. It has to be noted, however, that what we report here as the DWA results of Bartschat and Madison (1987, 1992b, 1995) and the RDWA results of Zuo *et al* (1991, 1992b) for r' do not include the contribution from excitation of the $6p[\frac{1}{2}]_1$ level to feature 4 since the above authors have not reported DCSs for excitation of that level. However, this contribution is small (less than 10%) according to UFOMBT results. We believe that the strong deviation of the present UFOMBT and UDWA results from the semirelativistic results of Bartschat and Madison (1995), comes from the fact that the latter authors used only the $5p^56s$ configuration contribution to the

wavefunctions while the present work also considered the $5p^55d$ configuration (as well as others). As one can see from table 1, the $5p^55d$ configuration provides a significant contributing term to the $6s[\frac{1}{2}]_1$ level wavefunction but practically no contribution to the $6s[\frac{3}{2}]_1$ level wavefunction. Further theoretical work would be desirable in this area.

The ratio r'' has been defined and determined for the purpose of dividing the combined scattering intensities for features 1 and 2 (and corresponding cross sections, DCS_{1+2}), obtained in low resolution measurements, into the proper DCS_1 and DCS_2 values. These ratios are also shown in figures 3 and 4 for $E_0 = 15$ and 30 eV, respectively. All four sets of experimental data for r'' (present, Khakoo *et al* 1994, Filipović 1988, Nishimura *et al* 1985, 1994) are in excellent agreement with each other except at 15 eV at small and large scattering angles. The general comments, regarding the theoretical values of r and r' , are also valid for the r'' results except that the DWA r'' results of Bartschat and Madison (1995) and the RDWA results of Zuo *et al* (1992b) are in better agreement with experiment than the UFOMBT results.

The ratio R_0^{1+2} , defined by equation (8), has been introduced for convenience in the normalization of the inelastic DCSs to the absolute scale. The combined scattering intensity represented by features 1 and 2 is conveniently determined in the ES experiments with high signal-to-noise ratio without the requirement for good energy resolution. The ES experiments can also conveniently produce the ratio of scattering intensities associated with this combined excitation with respect to elastic scattering. If the instrument detection efficiency were the same for electrons scattered elastically and inelastically, these ratios would represent the corresponding cross section ratios and in combination with available elastic DCSs would yield DCS_{1+2} , the inelastic DCS associated with combined features 1 and 2, which in turn could serve as a secondary standard for normalizing other inelastic DCSs. However, this is not the case in the ES measurements. The instrument response function depends on the residual energy of the scattered electron and a correction for this effect has to be introduced before we can derive the desired inelastic DCS_{1+2} values.

The TOF measurements yielded the correct DCS_{1+2}/DCS_0 ratios at 90° scattering angle at fixed impact energies and thus the correction factor in equation (8) which is applied to all scattering angles at that particular energy. At low impact energies (low residual energies) these ratios can be directly deduced from TOF spectra similar to those shown in figure 2. At impact energies of 15 eV or higher, this procedure becomes unreliable due to the decreasing timing resolution and heavy overlap from higher energy-loss features. At 15 and 20 eV incident electron energies, we deduced from the TOF spectra the ratio of the sum of the scattering intensity ratios for features 1 to 12 with respect to elastic scattering. At these energies, ES scattering measurements (at $\theta = 90^\circ$ and fixed E_0) were used to determine the relative contribution from excitation represented by combined features 1 and 2 to the overall inelastic scattering intensity for excitation represented by features 1 to 12 ($R_{1\text{ to }12}^{1+2}$). The combination of these two measurements then yielded the correct DCS_{1+2}/DCS_0 ratios based on equations (1) and (8). The pertinent results from these measurements are given in table 3 and figure 5. At $E_0 = 30$ eV the ES measurements can be relied on since the instrument detection efficiency for the elastic and inelastic scattering can be made very nearly the same.

5.2. Differential cross sections

The discussion of the DCSs will be separated according to features.

Combined features 1 and 2. These two features correspond to excitation of the metastable level $6s[\frac{3}{2}]_2$ (feature 1) and the $6s[\frac{3}{2}]_1$ level (feature 2), of which the latter is dipole coupled

to the ground state. The combined DCSs are discussed here because they were used by us to evaluate inelastic to elastic DCS ratios in the TOF measurements and because of the difficulty in resolving these two features. Furthermore, new and precise DCS_{1+2} values have been measured by Ester and Kessler (1994) as part of a program to carry out a 'perfect' electron scattering experiment on xenon. These combined DCSs serve as convenient and reliable secondary standards for normalizing the other inelastic DCSs.

Figure 6(a)–(c) shows DCSs associated with the combined features 1 and 2. At $E_0 = 15$ eV, all calculations predict reasonably correct shape but only the DWA of Bartschat and Madison (1995) yields the correct order of magnitude. At 20 and 30 eV, the theoretical results come closer to each other and to experiment. The situation improves as the impact energy is increased. This is the expected general trend for distorted-wave and first-order many-body theory type models and this was also found to be the case for similar comparisons with experiments in the case of He (Cartwright *et al* 1992, Trajmar *et al* 1992) and other rare gases (see e.g. Chutjian and Cartwright 1981, Trajmar *et al* 1981). Experimental results obtained by Ester and Kessler (1994) and Nishimura (1994) are, in general, in good agreement with present experimental results, but those of Filipović *et al* (1988) are considerably higher than ours.

Feature 1. This feature corresponds to excitation of the $6s[\frac{3}{2}]_2$ level and is weak compared to feature 2, especially in low-angle energy-loss spectra, and the corresponding DCSs are subject to rather large errors. In spite of this, the present and earlier experimental data are, in general, in good agreement with each other except for the values obtained by Filipović *et al* (1988) at 30 eV which are much larger. The theoretical results deviate significantly from the present experimental results at all impact energies. The experimental angular distributions are nearly isotropic at $E_0 = 10$ and 15 eV but some forward peaking character develops as the impact energy increases. As an example, the situation at $E_0 = 20$ eV is shown in figure 7. In our calculational scheme, the largest mixing coefficient of this $J = 2$ level eigenfunction is 0.9958 for the $5p^5 6s^3 P_2$ term, indicating that this level can be well characterized as a single configuration $^3 P_2$ level and, therefore, a nearly isotropic DCS behaviour is expected assuming that the excitation takes place predominantly through electron exchange as found at low impact energies.

Feature 2. This feature corresponds to excitation of the $6s[\frac{3}{2}]_1$ level which, in our calculational scheme, is characterized by dominant contributions from $^3 P_1$ and $^1 P_1$ terms. The largest mixing coefficients for this $J = 1$ level are 0.626 and 0.777 for the $5p^5 6s^3 P_1$ and $5p^5 6s^1 P_1$ terms, respectively. Because of the large contribution from the $^1 P_1$ component one expects large values for the DCSs and considerable forward peaking. The scattering intensity was indeed found to be strong and the relative DCSs could be determined with high accuracy.

DCS results at 15, 30, 50 and 80 eV impact energies are shown in figure 8(a)–(d), respectively. The experimental results are, in general, in agreement with each other except for those of Filipović *et al* (1988). Various theoretical models predict DCSs of about the same shape and magnitude and show better agreement with each other and with experiment as the impact energy increases.

At $E_0 = 50$ and 80 eV the semi-relativistic DWA results of Bartschat and Madison (1995) and the RDWA results of Zuo *et al* (1992b) are in excellent agreement with the experimental results (except at 80 eV for small scattering angles) and with each other, while the present UFOMBT and UDWA results agree with experiment up to about 50° of scattering angle. The deviation of the UFOMBT and UDWA results from the DWA and RDWA results at larger angles could be due to either (i) relativistic effects or (ii) the difference in the exchange potentials. We can hypothesize that the latter is more probable

since with increasing energy (going from 50 eV to 80 eV) the aforementioned deviation diminishes. This indicates that the exact exchange potential used by Zuo *et al* (1992b) and the Furness–McCarthy potential used by Bartschat and Madison (1995) are more accurate in this case than the semiclassical exchange potential used in the UFOMBT and UDWA calculation.

Feature 3. Feature 3 is associated with excitation of the $6s'[\frac{1}{2}]_0$ metastable level. The dominant term for this $J = 0$ level is $5p^56s^3P_0$, which has a mixing coefficient of 0.906, but there is significant contribution (coefficient = 0.413) from the $5p^55d^3P_0$ term which also has a drastic effect on the r parameter. The angular distribution of the DCSs is nearly isotropic at all impact energies except at 30 eV where a rather deep minimum develops at around 95° . The earlier results of Filipović *et al* (1988) agree, in general, with the present experimental results at $E_0 = 15$ and 20 eV but there are angular regions where the error bars do not overlap. At $E_0 = 30$ eV there are serious disagreements between the two experimental data sets. The theoretical results show poor agreement with experiment at these energies in shape and absolute value, although they are of the right order of magnitude. Since the major difference between the present UFOMBT and UDWA calculations and those of Bartschat and Madison (1992b, 1995) and Zuo *et al* (1992a, b) is the inclusion of the $5p^55d$ configuration into the basis set, one could conclude that the inclusion of this configuration into the basis set increases the cross section (at some energies substantially) for the excitation of this state. Representative examples for the DCS are given in figure 9(a) and (b) at 15 and 30 eV impact energies, respectively.

Feature 4. Feature 4 corresponds to the unresolved excitations to levels 4 and 5 which are designated as $6s'[\frac{1}{2}]_1$ and $6p[\frac{1}{2}]_1$, respectively (see table 1). For the $6s'[\frac{1}{2}]_1$ level wavefunction the dominant terms are $5p^56s^3P_1$, $5p^56s^1P_1$, and $5p^55d^3P_1$, with mixing coefficients of 0.715, 0.605, and 0.327, respectively. For the $6p[\frac{1}{2}]_1$ level wavefunction the dominant terms are $5p^56p^3S_1$, $5p^56p^3P_1$, and $5p^56p^1P_1$, with mixing coefficients of 0.861, -0.458 , and 0.208, respectively.

At 10 and 15 eV incident electron energy the combined DCSs are nearly isotropic but forward peaking character develops at the higher impact energies. The experimental results of Filipović *et al* (1988) are in good agreement with the present experimental results for this strong feature at 15 and 20 eV but not at 30 eV. The UFOMBT yields shapes similar to those obtained from experiment but approach the experimental results in magnitude only at higher impact energies. The theoretical results indicate that the major contribution to this feature comes from the $6p[\frac{1}{2}]_1$ level excitation, at all impact energies. The RDWA method of Zuo *et al* (1991, 1992b) yields good agreement with experiment at 20 and 30 eV (although the minor contribution from the $6s'[\frac{1}{2}]_1$ level was neglected). The DWA results of Bartschat and Madison (1987, 1992a, b, 1995) show better agreement with experiment than UFOMBT (but again the contribution from the $6s'[\frac{1}{2}]_1$ level excitation was not included in the DWA results).

Additional discussion on the comparison of experimental data with theoretical results can be found in Bartschat and Madison (1987, 1992a, b) and in Zuo *et al* (1991, 1992a).

6. Conclusion

The present measurements yielded the first inelastic DCSs at $E_0 = 10$ eV and improved DCSs at $E_0 = 15, 20$ and 30 eV. For the normalization of the present experimental DCSs a novel TOF calibration method was applied at the lower impact energies ($E_0 \leq 20$ eV). Good agreement with existing fragmentary experimental data has been found in general, although a factor of two disagreement exists at certain impact energies and scattering angles.

The present UDWA and UFOMBT calculations do not yield quantitatively correct DCSs at these low impact energies in general, although the shapes of the angular distributions are reasonably well predicted.

Nevertheless, the present theoretical results agree reasonably well with experimental data for optically allowed transitions for energies as low as 20 or 30 eV. Good agreement is found for the remaining transitions for $E_0 \geq 50$ eV. The UFOMBT results are closer to experiment than the UDWA results, which is usually the case for neutral species. Comparison of our theoretical results with those of Bartschat and Madison (1995) and Zuo *et al* (1992) suggest that the exchange potentials used in the latter two approaches may be better for agreement with experiment, in particular at large scattering angles. This hypothesis will be tested in future work.

The DCS ratios for the predominantly 3P_2 and 3P_0 levels (levels 1 and 3) are far away from the 5:1 statistical weight ratio, especially at lower impact energies. While none of the theoretical models discussed above yield reasonable predictions for these ratios, we have shown that inclusion of the $5p^55d$ configuration adds a significant contribution to the calculated values via configuration interaction.

Acknowledgments

The authors would like to thank Drs R E H Clark and J Abdallah Jr for help with the atomic structure and collisional excitation codes and for many useful discussions; and Drs H Nishimura, A Stauffer, D Madison and K Bartschat for supplying us with unpublished results. Financial support from the DOE-AUWI (for MAK), from NASA (for ST, LRL and IK) and from the DOE (for GC and CJF) is gratefully acknowledged.

References

- Abdallah J Jr, Clark R E H and Cowan R D 1988 *Los Alamos National Laboratory Manual* No LA-11436-M, vol I (unpublished)
- Bartschat K and Madison D H 1987 *J. Phys. B: At. Mol. Phys.* **20** 5839
- 1992a *J. Phys. B: At. Mol. Opt. Phys.* **25** 1361
- 1992b *J. Phys. B: At. Mol. Opt. Phys.* **25** 4619
- 1995 Private communication
- Cartwright D C, Csanak G, Trajmar S and Register D F 1992 *Phys. Rev. A* **45** 1602
- Chutjian A and Cartwright D C 1981 *Phys. Rev. A* **23** 2178
- Clark R E H 1978 *Comput. Phys. Commun.* **16** 119
- Clark R E H, Abdallah J Jr, Csanak G and Kramer S P 1989 *Phys. Rev. A* **40** 2935
- Clark R E H, Abdallah J Jr, Csanak G, Mann J B and Cowan R D 1988a *Los Alamos National Laboratory Manual* No LA-11436-M, vol II (unpublished)
- Clark R E H, Abdallah J Jr and Kramer S P 1988b *Los Alamos National Laboratory Manual* No LA-11436-M, vol III (unpublished)
- Clark R E H, Csanak G and Abdallah J Jr 1991 *Phys. Rev. A* **44** 2874
- Cowan R D 1968a *J. Opt. Soc. Am.* **58** 808
- 1968b *J. Opt. Soc. Am.* **58** 924
- 1981 *Theory of Atomic Spectra* (Berkeley, CA: University of California Press)
- Cowan R D and Griffin D C 1967 *J. Opt. Soc. Am.* **66** 1010
- Csanak G, Taylor H S and Yaris R 1971 *Phys. Rev. A* **3** 1322
- Cvejanović S, Comer J and Read F H 1974 *J. Phys. B: At. Mol. Phys.* **7** 468
- Ester T and Kessler J 1994 *J. Phys. B: At. Mol. Opt. Phys.* **27** 4295
- Filipović D, Marinković B, Pejčev V and Vusković L 1988 *Phys. Rev. A* **37** 356
- Fontes C J, Clark R E H, Abdallah J Jr, Csanak G, Trajmar S, Khakoo M A and Kanik I 1996 *Los Alamos National Laboratory Report* in preparation
- Holtkamp G 1981 *Diploma Thesis* University of Münster

- Inal M K and Dubau J 1987 *J. Phys. B: At. Mol. Phys.* **20** 4221
- Khakoo M A, Beckmann C E, Trajmar S and Csanak G 1994 *J. Phys. B: At. Mol. Opt. Phys.* **27** 3159
- Khakoo M A and Trajmar S 1986 *Phys. Rev. A* **34** 138
- Khakoo M A, Trajmar S, Wang S, Kanik I, Aguirra A, Fontes C J, Clark R E H and Abdallah J Jr 1996 *J. Phys. B: At. Mol. Opt. Phys.* **29** 3477
- Khakoo M A, Tran T D, Bordelon D and Csanak G 1992 *Phys. Rev. A* **45** 219
- LeClair L R, Trajmar S, Khakoo M A and Nickel J 1996 *Rev. Sci. Instrum.* **67** 1753
- Mann J B 1983 *At. Data Nucl. Data Tables* **29** 407
- Moore C E 1957 *Atomic Energy Levels* vol 3 (NSRDS-NBS Publication 35) (Washington, DC: US Govt Printing Office)
- Nickel J, Zetner P W, Shen G and Trajmar S 1989 *J. Phys. E: Sci. Instrum.* **22** 730
- Nishimura H 1994 Private communication
- Nishimura H, Danjo A and Matsuda T 1985 *Proc. 14th Int. Conf. on the Physics of Electronic and Atomic Collisions (Palo Alto)* Abstracts p 108
- Nishimura H, Matsuda T and Danjo A 1987 *J. Phys. Japan* **56** 70
- Novgorodov A I 1974 *Investigation of Plasmas of Molecular Lasers* ed N G Basov (Moscow: USSR Academy of Sciences) p 105
- Register D F, Vušković L and Trajmar S 1986 *J. Phys. B: At. Mol. Phys.* **19** 1685
- Rhodes C K 1983 *Excimer Lasers (Topics in Applied Physics 30)* 2nd enlarged edn (New York: Springer)
- Saraph H E 1972 *Comput. Phys. Commun.* **3** 256
- Tawara H and Phaneuf R A 1988 *Comment. At. Mol. Phys.* **21** 177
- Trajmar S, Register D F, Cartwright D C and Csanak G 1992 *J. Phys. B: At. Mol. Opt. Phys.* **25** 4889
- Trajmar S, Srivastava S K, Tanaka H, Nishimura H and Cartwright D C 1981 *Phys. Rev. A* **23** 2167
- Veerasingam R *et al* 1995 *48th Gaseous Electronics Conf. Bull. Am. Phys. Soc.* **40** 1583
- Weyhreter M, Barzick B, Mann A and Linder F 1988 *Z. Phys. D* **7** 333
- Williams W, Trajmar S and Kupperman A 1975 *J. Chem. Phys.* **62** 3031
- Williamson W, Drallos P J and Nagorny V P 1994 *SPIE* **2174** 163
- Zuo T, McEachran R P and Stauffer A D 1991 *J. Phys. B: At. Mol. Opt. Phys.* **24** 2853
- 1992a *J. Phys. B: At. Mol. Opt. Phys.* **25** 3393
- 1992b Private communication